ACS OMEGA

Article

Cite This: ACS Omega 2019, 4, 1982−1994

http://pubs.acs.org/journal/acsodf

Enhanced Removal of Veterinary Antibiotic Florfenicol by a Cu-Based Fenton-like Catalyst with Wide pH Adaptability and High Efficiency

Ting Chen,[†,§] Zhiliang Zhu,[*,†,§] Hua Zhang,[†] Xiaolin Shen,[†,§] Yanling Qiu,[‡,§] and Daqiang Yin[‡,§]

[†]State Key Laboratory of Pollution Control and Resource Reuseand [‡]Key Laboratory of Yangtze River Water Environment, Ministry of Education, Tongji University, Shanghai 200092, China

[§]Shanghai Institute of Pollution Control and Ecological Safety, Shanghai 200092, China

Supporting Information

ABSTRACT: The study on the removal of refractory veterinary antibiotic florfenicol (FF) in water is still very limited. In this study, an efficient Fenton-like catalyst was developed by synthesizing a series of Cu-based multi-metal layered double hydroxides (CuNiFeLa-LDHs) to degrade FF in aqueous solution. In the experiments, the screened CuNiFeLa-2-LDH with the molar ratio of $La^{3+}/(Fe^{3+} + La^{3+})$ = 0.1 exhibited high catalytic activity, achieving almost complete degradation of 5 mg L^{-1} FF under 5 mmol L^{-1} H_2O_2 conditions. The mechanisms revealed that the enhanced catalytic performance was ascribed to the existence of Ni which accelerated the electron transfer rate and La which served as a Lewis acidic site to provide more reactive sites in this Cu-dominated Fenton-like reaction, further generating $^{\bullet}OH$, $^{\bullet}O_2^-$, and O_2^1 as active species to attack pollutants directly. Interestingly, the catalyst showed a wide pH adaptability and little release of copper ions to the solution. The regenerated CuNiFeLa-2-LDH is demonstrated to be a stable and reliable material for florfenicol degradation.

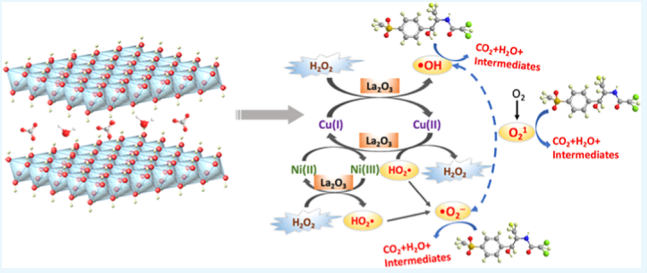

1. INTRODUCTION

Veterinary antibiotics (VAs), as a category of pharmaceuticals, are used widely for the disease precaution of animals in many countries.[1] It was estimated that the average usage of VAs in China has reached about 6000 metric tons per year with continuous growth.[2] The discharged antibiotics may enter the soil through land application of manures in the farmland and further release into the aquatic environment by runoff, driftage, or leaching.[3,4] In recent years, researchers have evidenced that the presence of antibiotics and antibiotic resistance genes in wastewater have a great possibility to disturb the natural ecological balance and result in an increase of resistant bacteria in the natural environment, posing a serious threat to ecosystems and human health.[5,6] Among these VAs, florfenicol (FF) is a synthetically produced broad-spectrum antibacterial agent and is especially developed for veterinary application.[7] As one of the few allowed VAs in aquaculture, FF can exist for a long time in the environment and traditional water treatment technologies cannot effectively degrade or remove it.[8] Numerous approaches have been employed to solve the pollution of antibiotics, such as photocatalysis, adsorption and biodegradation.[9−11] However, studies on the degradation of refractory VAs, especially FF, are still limited.

The Fenton reaction, as one of the most efficient advanced oxidation processes, has attracted more attention for the removal of antibiotics from water in recent years.[12,13] Generally, the generation of active species ($^{\bullet}OH$, $^{\bullet}O_2^-$, etc.) between Fe^{2+} and H_2O_2 can oxidize and mineralize pollutants into harmless substances such as CO_2 and H_2O.[14] However, the application of the classical homogeneous Fenton reaction is limited due to the requirement of low pH (<4), the difficulty of Fe^{2+}/Fe^{3+} cycling, and the production of ferric hydroxide sludge in aqueous solution.[15,16] To avoid the above disadvantages, the heterogeneous Fenton-like reaction was developed to degrade organic pollutants efficiently in a possible wide pH range. Among these improved methods, it has been observed that copper has the same Fenton reaction effect as iron. As expected, Cu^+ can be oxidized by H_2O_2 to produce $^{\bullet}OH$. The oxidized state of Cu^{2+} can react with H_2O_2 to generate $HO_2^{\bullet}$ (eqs 1 and 2). The circulation rate of Cu^+/Cu^{2+} is much faster than Fe^{2+}/Fe^{3+} (eqs 3 and 4), loosening the limited rate step.[16,17] Moreover, copper has good pH adaptability, which is proved to be a significant advantage for the replacement of iron in the Fenton reaction.

$$Cu^+ + H_2O_2 \rightarrow Cu^{2+} + {}^{\bullet}OH + OH^-,\ k_1 = 1 \times 10^4\ M^{-1}S^{-1} \quad (1)$$

Received: December 4, 2018
Accepted: January 11, 2019
Published: January 25, 2019

DOI: 10.1021/acsomega.8b03406
ACS Omega 2019, 4, 1982−1994

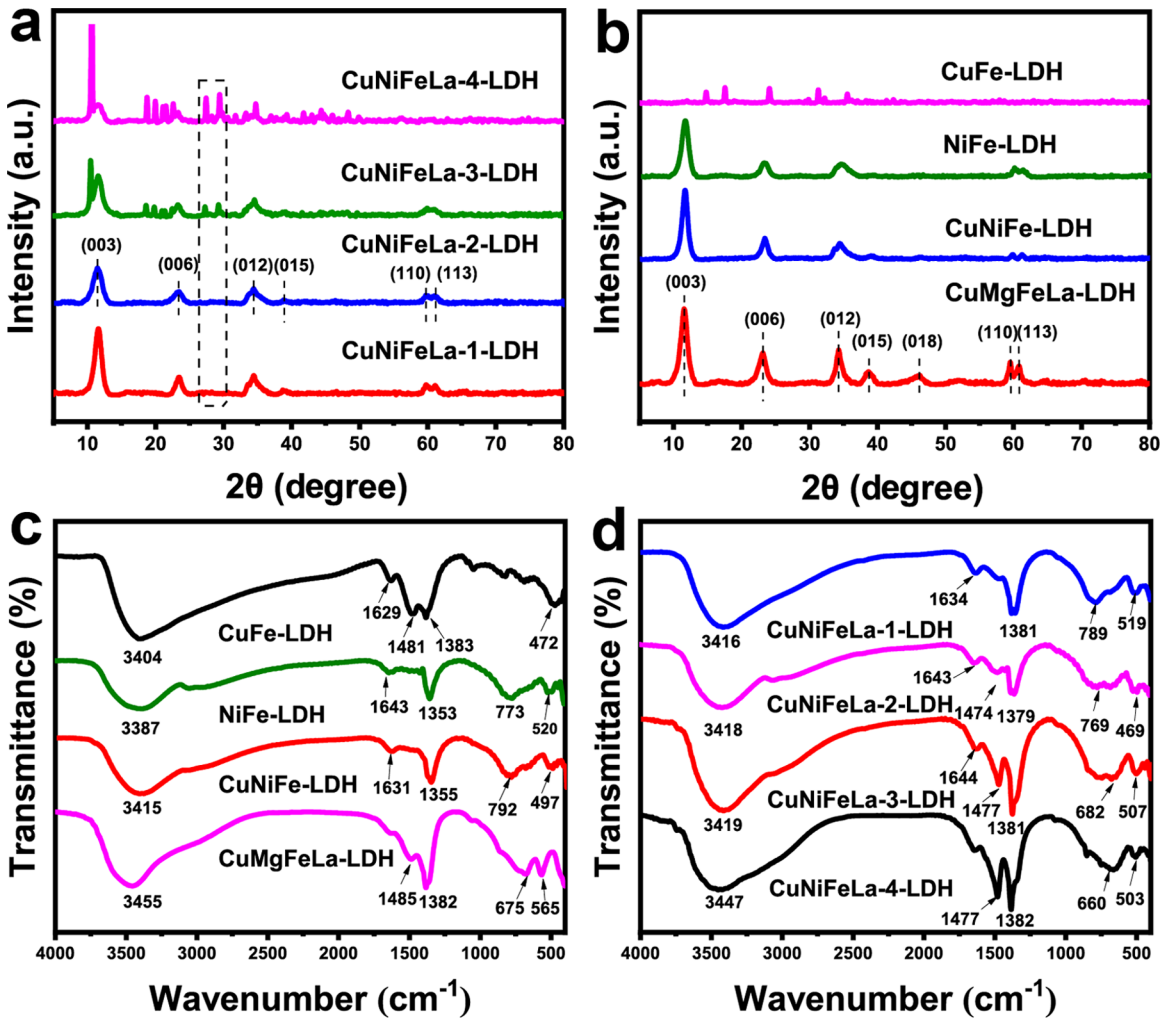

Figure 1. XRD patterns of (a) different La-doped CuNiFeLa-LDHs, (b) CuFe-LDH, NiFe-LDH, CuNiFe-LDH, and CuMgFeLa-LDH, respectively. Fourier transform infrared (FTIR) patterns of (c) CuFe-LDH, NiFe-LDH, CuNiFe-LDH, and CuMgFeLa-LDH, (d) different La-doped CuNiFeLa-LDHs, respectively.

$$Cu^{2+} + H_2O_2 \rightarrow Cu^{+} + HO_2^{\bullet} + H^{+},\ k_2 = 4.6 \times 10^2\ M^{-1}S^{-1} \quad (2)$$

$$Fe^{2+} + H_2O_2 \rightarrow Fe^{3+} + {}^{\bullet}OH + OH^{-},\ k_3 = 76\ M^{-1}S^{-1} \quad (3)$$

$$Fe^{3+} + H_2O_2 \rightarrow Fe^{2+} + HO_2^{\bullet} + H^{+},\ k_4 = (0.1 - 2) \times 10^{-2}\ M^{-1}S^{-1} \quad (4)$$

To avoid the mobilization of Cu^{+}/Cu^{2+} in aqueous solution, numerous methods have been suggested to load copper onto the solid substrate to remove different organic pollutants, such as Cu-based bimetallic oxides, Cu-doped goethite, and the zero-valent iron/Cu bimetallic catalyst.[18−20] Layered double hydroxides (LDHs), with the general formula $[M_{1-x}^{2+}M_x^{3+}(OH)_2]^{x+}(A^{n-})_{x/n}\cdot mH_2O$, where M^{2+} and M^{3+} represent divalent and trivalent metal cations, respectively, has certified a category of catalyst and adsorbent to purify the polluted water. Due to the excellent properties, such as anionic exchangeability, topotactic transformation, the high specific surface area, and the typical lamellar structure, LDH materials have attracted attention from researchers in recent years.[21−23] Previous studies including our research group have investigated the Fenton effect of Cu-LDHs, illustrating the possibility of Cu-LDH used in catalytic oxidation to degrade organic pollutants in water.[24−26] However, few studies have reported about the effects of cation compositions in LDHs on the Fenton-like reaction.

The objective of this study was to develop a novel Cu-based multi-metal material CuNiFeLa-LDH used as the Fenton-like catalyst with a wide pH adaptability and low release of heavy metal ions to purify the polluted water containing the refractory VAs, FF. To compare the performances of CuNiFeLa-LDH with other related LDH materials and explore the contribution of different compositions, several LDHs including CuFe-LDH, NiFe-LDH, CuNiFe-LDH, and CuMgFeLa-LDH were prepared. The influence of different factors such as La doping contents, H_2O_2 concentration, catalyst dosage, and FF concentrations were investigated. Several antibiotics such as ibuprofen (IBF), diclofenac sodium (DCF), and paracetamol (PR) were also used as pollutants to evaluate the applicability of the material. In addition, the reusability and stability of the material was evaluated by regenerating the catalyst of each cycle. The possible promotion mechanism of La and Ni in CuNiFeLa-LDH on degradation of FF by the heterogeneous Fenton-like reaction was proposed and

DOI: 10.1021/acsomega.8b03406
ACS Omega 2019, 4, 1982−1994

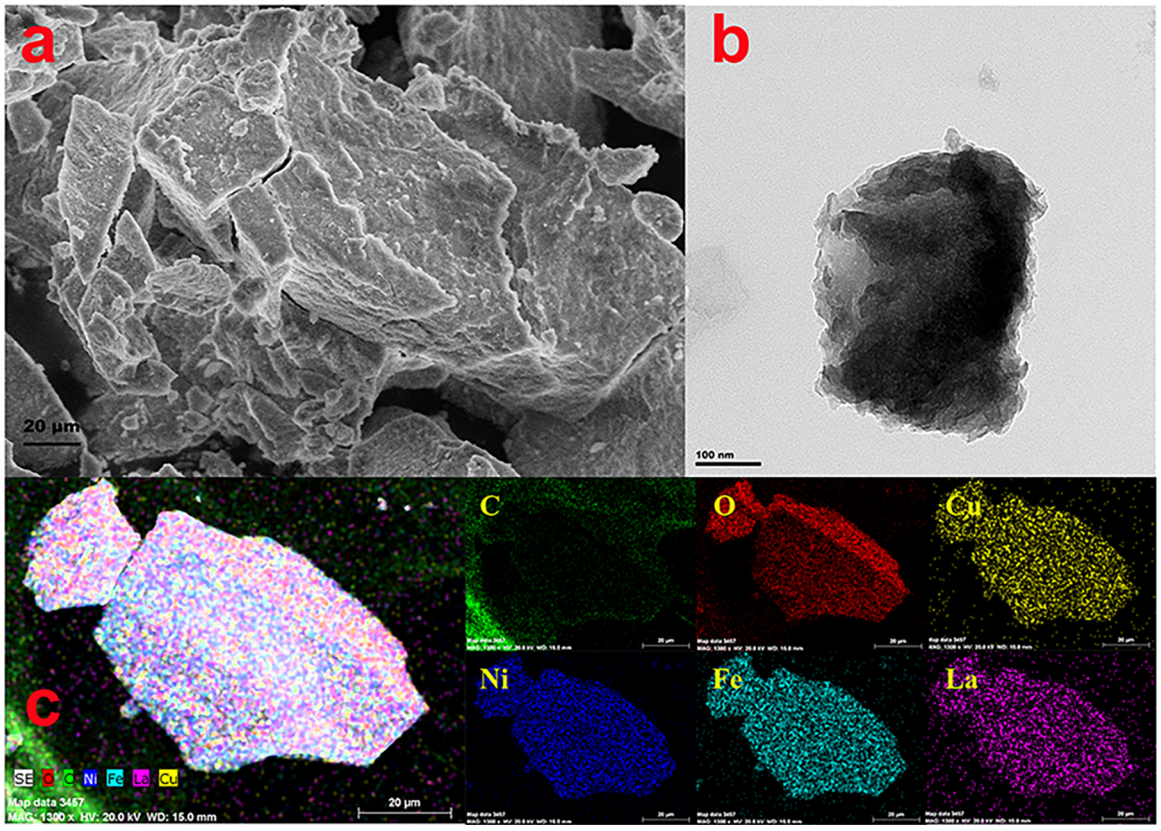

Figure 2. (a) SEM image, (b) TEM image, (c) elemental mapping analysis of CuNiFeLa-2-LDH.

discussed by a series of experiments before and after the reaction.

2. RESULTS AND DISCUSSION

2.1. Characterization. *2.1.1. Chemical Composition of Synthesized Materials.* The material, CuNiFeLa-LDH, with a fixed content of La doping was dissolved in a certain concentration of concentrated nitric acid and the content of metal ions was measured by inductively coupled plasma optical emission spectrometry (ICP-OES). The chemical compositions of the materials are presented in Table S1. It is clearly found that the results of CuNiFeLa-LDHs were consistent with the molar ratio of the initial synthesis. Considering the general formula, the chemical compositions of the materials were calculated.

2.1.2. X-ray Diffraction (XRD) Analysis. The XRD patterns of the synthesized CuNiFeLa-LDHs with different La doping contents are shown in Figure 1a. It is obviously observed that CuNiFeLa-LDH materials maintained a good crystal structure with lower La doping contents. The crystallographic planes of (003), (006), (012), (015), (110), and (113) represented the typical diffraction peaks of LDHs.[27−29] However, the intensity of the diffraction peaks decline, indicating that the layered hydrotalcite-like structure was destroyed with the addition of more La proportion. The changes were attributed to excessive introduction of numerous large ionic radius of La^{3+} species, which can attract more carbonate ions into the lattice and result in poor crystallinity of the materials.[30] In addition, two diffraction peaks for La_2O_3 in the range of 25−30° appear in CuNiFeLa-3-LDH and CuNiFeLa-4-LDH instead of CuNiFeLa-1-LDH and CuNiFeLa-2-LDH, which proved that a small amount of La doping did not affect the LDH crystallization.[31]

For comparative analysis, the XRD patterns of several different metal cation compositions in LDHs are given in Figure 1b. It can be found that NiFe-LDH, CuNiFe-LDH, and CuMgFeLa-LDH exhibit similar diffraction peaks, whereas the layered structure disappears in CuFe-LDH when Cu^{2+} and Fe^{3+} entered into the laminate. This could be explained by Jahn−Teller distortion, which can increase the disorder of the crystallization of the laminate.[32]

2.1.3. FTIR Analysis. The surface functional groups of the materials were characterized by FTIR spectra. Figure 1c depicts the FTIR spectrum of the as-prepared CuNiFeLa-LDHs with different La doping contents. These spectra are consistent with the typical FTIR patterns of LDHs.[33] Moreover, the introduction of the rare earth element La to the lattice can slightly change the peak shift. Among these spectra, the strong and broad adsorption peak near 3418 cm^{-1} of all samples can be assigned to the O−H stretching vibrations from hydroxyl groups and interlayer water molecules. The bending vibration band of water molecules appear around 1643 cm^{-1}. In addition, the intensity of the adsorption peak at 1380 cm^{-1} ($\nu_3(CO_3^{2-})$) and 1477 cm^{-1} ($\nu_3(CO_3^{2-})_{ads}$) is strengthened with the enlargement of lanthanum doping for the attraction of carbon dioxide, resulting in an increase of carbonate anions in the interlayer to maintain charge balance.[34,35] The increased carbonate anions can result in the enlargement of the interlayer spacing, making it easier for contaminants to contact with the material for the degradation process. The peaks in the low frequency area of wavenumber from 400 to 800 cm^{-1} corresponded to the lattice vibration such as metal−oxygen−metal (M−O−M) stretching and metal-hydroxyl vibrations. For comparison, the FTIR patterns of other LDHs are given in Figure 1d. The O−

DOI: 10.1021/acsomega.8b03406
ACS Omega 2019, 4, 1982−1994

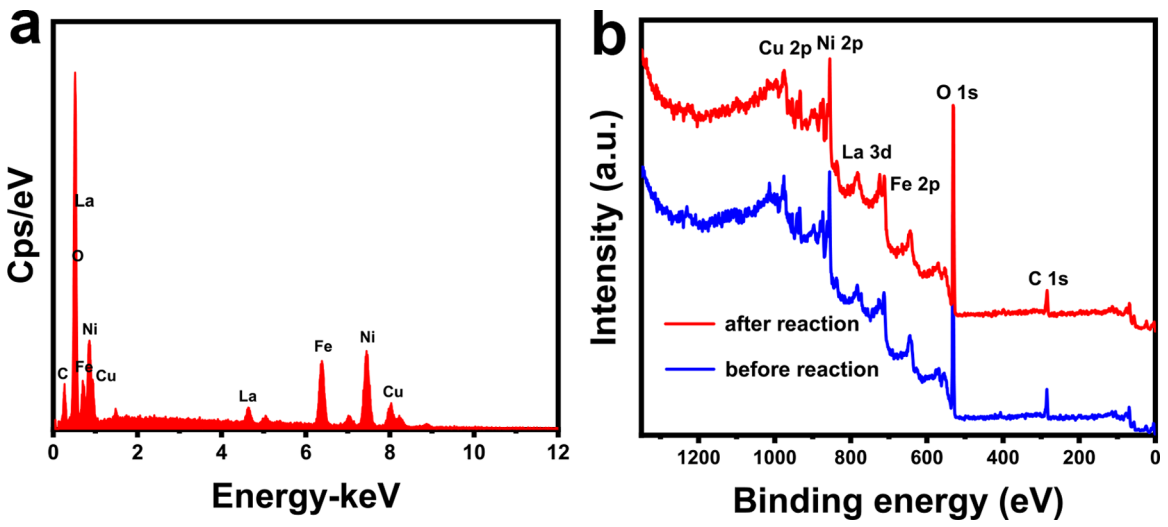

Figure 3. (a) EDS analysis results of CuNiFeLa-2-LDH, (b) full X-ray photoelectron spectroscopy (XPS) spectrum of CuNiFeLa-2-LDH before and after the reaction.

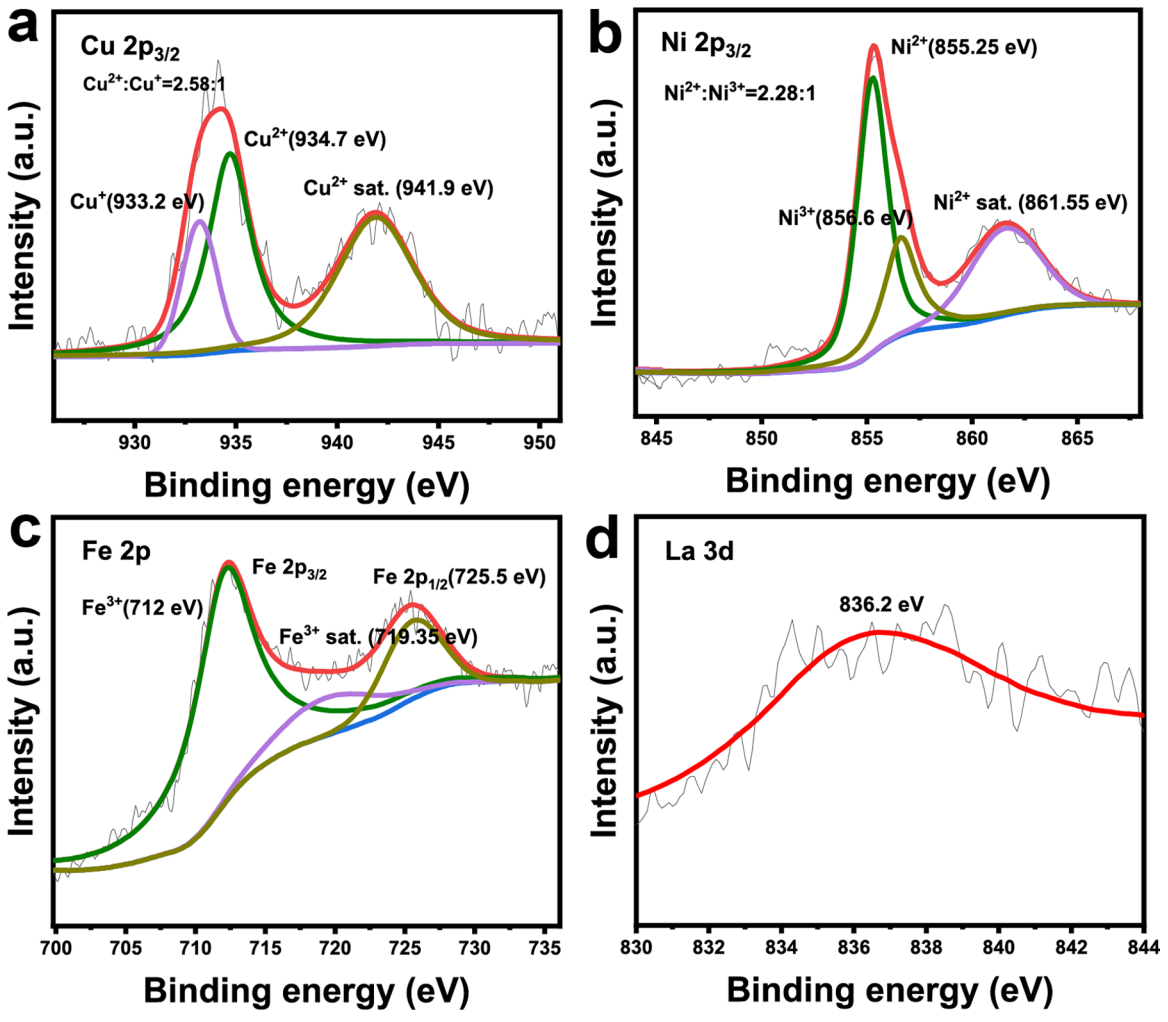

Figure 4. High-resolution XPS spectrum of CuNiFeLa-2-LDH (a) Cu 2p, (b) Ni 2p, (c) Fe 2p, and (d) La 3d before the reaction.

H stretching vibrations, H_2O bending vibrations, stretching of CO_3^{2-}, and M−O−M vibration of all samples can be found, which resembled those of other LDHs.[36,37]

2.1.4. Brunauer−Emmett−Teller (BET) and ζ-Potential Analysis. The N_2 adsorption−desorption isotherms and pore size distribution of CuNiFe-LDH and CuNiFeLa-2-LDH are shown in Figure S1. The specific surface area was calculated from the adsorption data by the Brunauer−Emmett−Teller (BET) method, whereas the total pore volume and pore size distribution was analyzed from the desorption branch by the

DOI: 10.1021/acsomega.8b03406
ACS Omega 2019, 4, 1982−1994

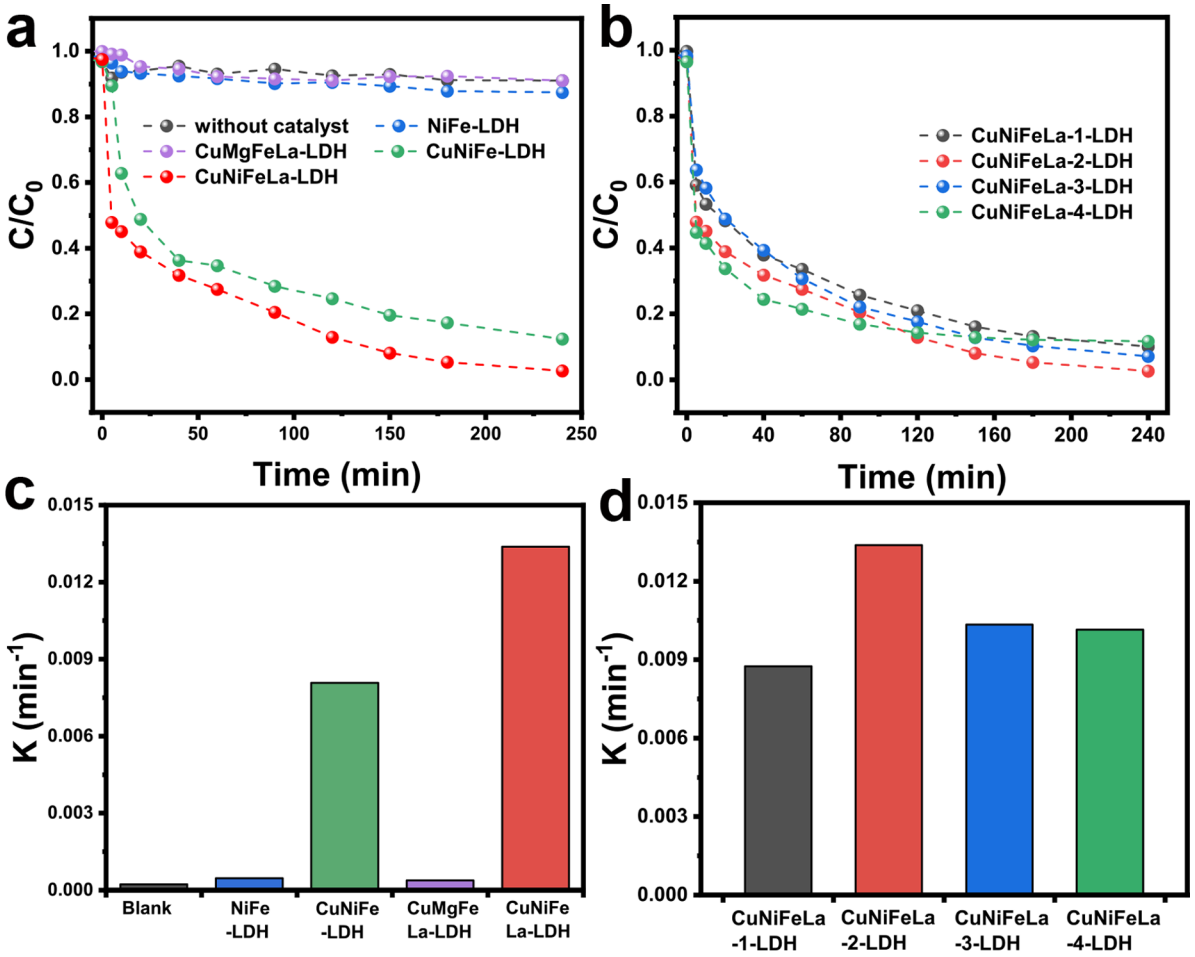

Figure 5. Heterogeneous Fenton-like performance of (a) different LDHs, (b) different La-doped CuNiFeLa-LDHs on the degradation of FF. The FF degradation rate constants of (c) different LDHs, (d) different La-doped CuNiFeLa-LDHs. Conditions: [H_2O_2] = 5 mmol L^{-1}, [catalyst] = 0.25 g L^{-1}, [FF] = 10 mg L^{-1}, natural pH.

Brunauer–Joyner–Halenda method. It is observed that both CuNiFe-LDH and CuNiFeLa-2-LDH displayed type IV isotherms with a H3 type hysteresis loop according to the IUPAC classification. In addition, CuNiFe-LDH has the pore size distribution between 2 and 15 nm, whereas CuNiFeLa-2-LDH shows the uniform distribution due to the existence of mesopores, which demonstrated that the doping of La can fabricate more mesopores in the material, making the entrance of FF into the sample for degradation more easy. The specific surface area of CuNiFeLa-2-LDH (162.823 m^2 g^{-1}) is much higher than that of CuNiFe-LDH (82.899 m^2 g^{-1}), which is essential for FF degradation to provide more active sites. The ζ-potential of CuNiFeLa-2-LDH is 8.61, measured in the pH range from 6 to 10 as shown in Figure S2.

2.1.5. Surface Morphology Analysis. An scanning electron microscopy (SEM) image of CuNiFeLa-2-LDH is presented in Figure 2a. As can be seen from the image, the sample shows a plate-like morphology and the materials are aggregated. The transmission electron microscopy (TEM) image of CuNiFeLa-2-LDH exhibits a layered structure in Figure 2b. The area with saturated color manifested that the thick plate-like structure was aggregated, which can be ascribed to the introduction of La^{3+} for the effect of the crystallinity of LDHs and the aggregation of the lattice. In addition, the elemental mapping analysis (Figure 2c) of CuNiFeLa-2-LDH confirmed that the elements Cu, Ni, Fe, and La were highly dispersed within the laminate, and the appearance of C and O indicated that this LDH intercalated with carbonate anions. Besides, the energy dispersive spectrum (EDS) of CuNiFeLa-2-LDH is given in Figure 3a. The peaks of this material further certified the presence of the metal elements which insert into the lattice. The molar ratio between the metal elements is consistent with that measured by ICP-OES (Table S2).

2.1.6. XPS Analysis. The full XPS spectrum of the sample is presented in Figure 3b. In the typical XPS survey, all elements in this LDH material were detected. The peaks of C 1s and O 1s are shown in Figure S3. The high-resolution of the Cu $2p_{3/2}$ transition of the sample are shown in Figure 4a. The "shake-up" peak of the Cu^{2+} satellite is obviously observed at the binding energy of 941.9 eV. The peak at 934.7 eV corresponded to the oxidation of copper species (Cu^{2+}), whereas the peak located at 933.2 eV exhibited the reduction copper species (Cu^{+}) according to previous reports,[38,39] and the ratio of Cu^{2+}/Cu^{+} equals to 2.58:1. These results signified that both Cu^{+} and Cu^{2+} existed on the surface of CuNiFeLa-2-LDH and the efficiency of the Fenton-like reaction might be regulated by the cycle of Cu^{+}/Cu^{2+}. In Ni $2p_{3/2}$ spectra, their characteristic peaks are discovered as presented in Figure 4b. The appearance of a shake-up satellite line at 861.55 eV was attributed to Ni^{2+} on the surface of the catalyst. Besides, the peak at 856.6 eV confirmed the oxidation of nickel species belonging to Ni^{3+} and that near 855.25 eV corresponded to the

DOI: 10.1021/acsomega.8b03406
ACS Omega 2019, 4, 1982−1994

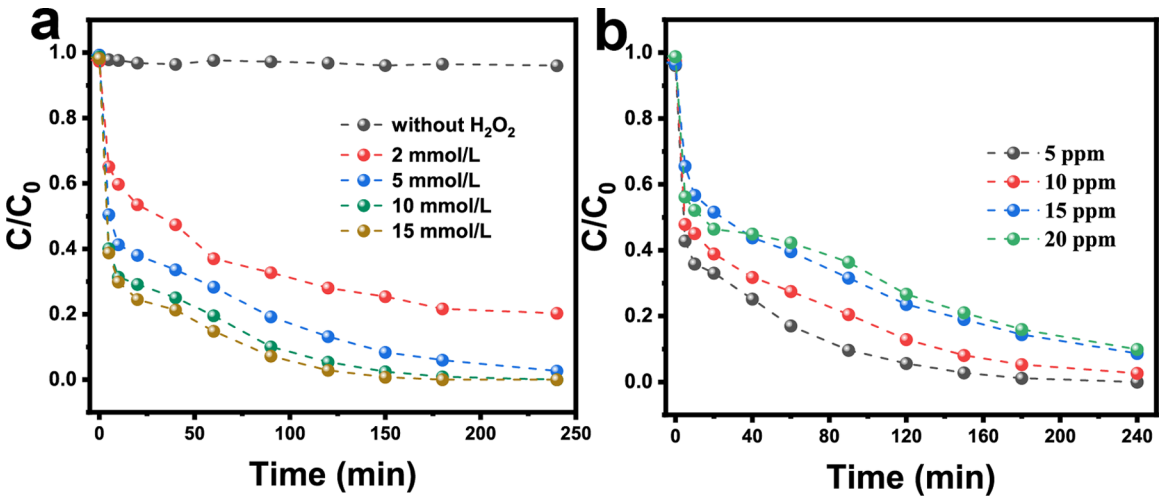

Figure 6. Influence factors of (a) H_2O_2 concentration, (b) FF concentration.

reduction state of nickel species (Ni^{2+}).[40] The XPS curve fittings of nickel species manifested the existence of Ni^{2+} and Ni^{3+} with the atomic ratio of 2.28:1, indicating that the electron transfer process may occur. In addition, the peaks of Fe 2p and La 3d were also measured as shown in Figure 4c,d, which illustrated the existence of Fe^{3+} and La_2O_3.[41,42]

Combining the above facts, the electron transfer between copper and nickel is surmised in this Fenton-reaction system. The existence of Ni^{2+} with the valence electronic configuration $3d^64s^2$ is regarded as the electron donor to reach a state of half-full electronic configuration, whereas Cu^{2+} with the valence electronic configuration $3d^9$ is considered as the electron acceptor to form the stable valence electronic structure. This suggests that Ni^{2+} probably provides an electron to Cu^{2+} through the lattice oxygen in the LDH interlayers.

2.2. Heterogeneous Fenton-like Performance. *2.2.1. Effect of Different Compositions in Cu-LDHs.* The Fenton-like performance of different materials was evaluated by the degradation of FF under dark conditions. As seen in Figure 5a, the catalytic activity of different metal cation compositions in Cu-LDHs was investigated. The results clearly revealed that CuNiFeLa-LDH exhibited the best Fenton-like reactivity among these LDHs. Compared to CuNiFe-LDH, the introduction of La^{3+} can enhance the degradation of FF, indicating that the element La can improve the degradation efficiency in the Fenton-reaction system. The degradation rate of FF by CuFe-LDH was fast in the first 5 min. However, it almost remained unchanged after 10 min for the collapse of brucite-like layers of CuFe-LDH and increased the consumption of the active species. Besides these, the concentration of FF remained nearly unchanged with the presence of NiFe-LDH or CuMgFeLa-LDH. A blank experiment without catalysts was also executed to prove that FF was scarcely degraded with the absence of catalysts. The apparent rate constants of different materials can be calculated and the values are exhibited in Figure 5c. The results signified that CuNiFeLa-LDH possessed the highest Fenton-like reactivity with the apparent rate constant k_{app} = 0.01338 min^{-1}. According to these facts, the high efficiency of FF degradation can be speculated as the coexistence of Cu and Ni, which might activate the catalytic activity of the material due to the unique valence electronic structures of these two metal ions. The doping of La can fabricate more mesopores in the material and contribute both base and acid properties in the reaction system, which can enhance the removal efficiency in our experiment.[43]

2.2.2. Effect of La Contents in CuNiFeLa-LDH. The optimum content of La dopants in CuNiFeLa-LDHs in the Fenton-like reaction was evaluated as shown in Figure 5b. It presented that the optimum catalytic reactivity of CuNiFeLa-LDH is with the molar ratio up to 0.1 (La^{3+}/Fe^{3+} + La^{3+}). However, excessive La dopants can cause collapse of the layered structure according to XRD analysis, resulting in the reduction of reactive sites. The apparent rate constants demonstrated that CuNiFeLa-2-LDH has the higher catalytic reactivity (k_{app} = 0.01338 min^{-1}) than other La dopants (Figure 5d).

2.2.3. Influence Factors. The influence factors in the heterogeneous Fenton-like reaction of CuNiFeLa-2-LDH was evaluated. The concentration of H_2O_2 on the degradation of FF is shown in Figure 6a. It turned out that the removal rate of FF was enhanced with the increase of the H_2O_2 concentration. The improved degradation rate was attributed to the more amount of H_2O_2 that reacted with the catalyst to promote the production of active species. The effect of the initial FF concentration was investigated with the concentration from 5 to 20 mg L^{-1}. As depicted in Figure 6b, FF in solution after the treatment was not detected by ultraperformance liquid chromatography (UPLC) (detection limit: 50 μg L^{-1}) with the initial concentration of 5 mg L^{-1} after 180 min, basically achieving almost complete degradation under a low dosage of H_2O_2 conditions. However, the removal rate decreased with the increase of the FF concentration for the limited active sites at the given dosage of the catalyst. Figure S4 shows the effect factor of the catalyst dosage from 0.25 to 1.0 g L^{-1} on the degradation of FF. It was clearly observed that the degradation rate of FF was slightly improved with the increase of the catalyst dosage. In other words, a small amount of catalyst exhibited a good Fenton-like catalytic effect under experimental conditions.

2.3. Degradation of Other Antibiotics by CuNiFeLa-LDH. To verify that CuNiFeLa-LDH is suitable for the degradation of other antibiotics, the same removal procedure of IBF, DCF, and PR were implemented. From Figure 7, the result showed that the removal efficiency can reach over 95% of the three antibiotics after 180 min. This indicates that

DOI: 10.1021/acsomega.8b03406
ACS Omega 2019, 4, 1982−1994

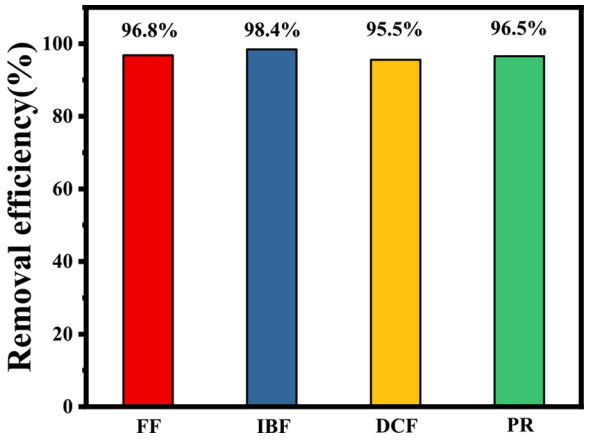

Figure 7. Degradation of FF, IBF, DCF, and PR by CuNiFeLa-2-LDH. Conditions: [H_2O_2] = 5 mmol L^{-1}, [catalyst] = 0.25 g L^{-1}, [antibiotics] = 10 mg L^{-1}, natural pH.

CuNiFeLa-LDH can be used to degrade different pollutants in aqueous solution with applicability.

2.4. Reusability and Stability of CuNiFeLa-LDH. The reusability and stability of the catalyst are crucial for its practical application. The five cycling tests of CuNiFeLa-2-LDH were carried out with the same reaction procedure on the degradation of FF. As shown in Figure 8a, the catalytic activity of CuNiFeLa-2-LDH did not obviously decrease at the end of repeated five runs. Figure 3b displays the full XPS spectrum of CuNiFeLa-2-LDH before and after the reaction. The spectra show similar XPS patterns and the elements Cu, Ni, Fe, La, C, and O were still included, which demonstrated that there is little change in elemental composition over the sample after the reaction. Interestingly, only 0.229 mg L^{-1} Cu was detected after the reaction. It is much lower than the regulation of EU (<2 mg L^{-1}) and USA (<1.3 mg L^{-1}), indicating that it is a stable material used as a Fenton-like catalyst on the degradation of pollutants.

To explore the environmental adaptability of the material, the initial pH value of FF solution was considered with the pH changing from 5.0 to 9.0. As described in Figure 8b, the initial pH value exhibited little influence on the degradation rate, indicating that CuNiFeLa-2-LDH has a good degradation effect for FF over a wide pH range. The inserted figure shows the data for pH change during the degradation process. As shown in the results, regardless of different initial pH values, it eventually tended to the similar neutral pH range. In a way, it proved that this material possessed satisfied pH adaptability in aqueous solution and circumvented the requirement of low pH values in the traditional Fenton reaction. Therefore, these results evidenced that CuNiFeLa-2-LDH was a stable and reliable Fenton-like material under the experimental conditions.

2.5. Catalytical Mechanisms. Generally, reactive oxygen species (ROS) in the Fenton-like reaction system always act as the main active substances to oxidize organics and achieve the purpose of degradation and mineralization of pollutants in the heterogeneous Fenton-like process.[44,45] To clarify the contributions of each ROS for the degradation of FF using CuNiFeLa-2-LDH, the scavenger experiments of O_2^1, $^{\bullet}O_2^-$, and $^{\bullet}OH$ were implemented using NaN_3, BQ, and TBA, respectively, under different concentration gradients. Figure 9a illustrates the results of each scavenger for the degradation of FF over CuNiFeLa-2-LDH. The degradation efficiency of FF was ~96.8% without the scavenger. However, a phenomenon of dramatic decrease of the removal rate occurred after the three scavengers with high concentrations were added separately. Compared with the absence of scavengers, the removal rates were reduced by 92.4, 91.6, and 90.3%, respectively. The accession of NaN_3, BQ, and TBA with the concentration from 0.01 to 5 mmol L^{-1} obstructed the reaction between the catalyst and H_2O_2 in some degree, apparently manifesting that the inhibitory effect on degradation of FF was significant with the increase of scavengers. These above phenomena indicated two facts: (1) the three ROS O_2^1, $^{\bullet}O_2^-$, and $^{\bullet}OH$ were involved in the reaction system and played important roles in the degradation of FF, (2) the actuality of the addition of one capture agent with a high concentration inhibited the entire reaction, demonstrating the interaction among the three active species during the process.

To further directly detect the generation of ROS in the experimental procedure, the DMPO-trapped ESR technique was employed with and without CuNiFeLa-2-LDH or H_2O_2.

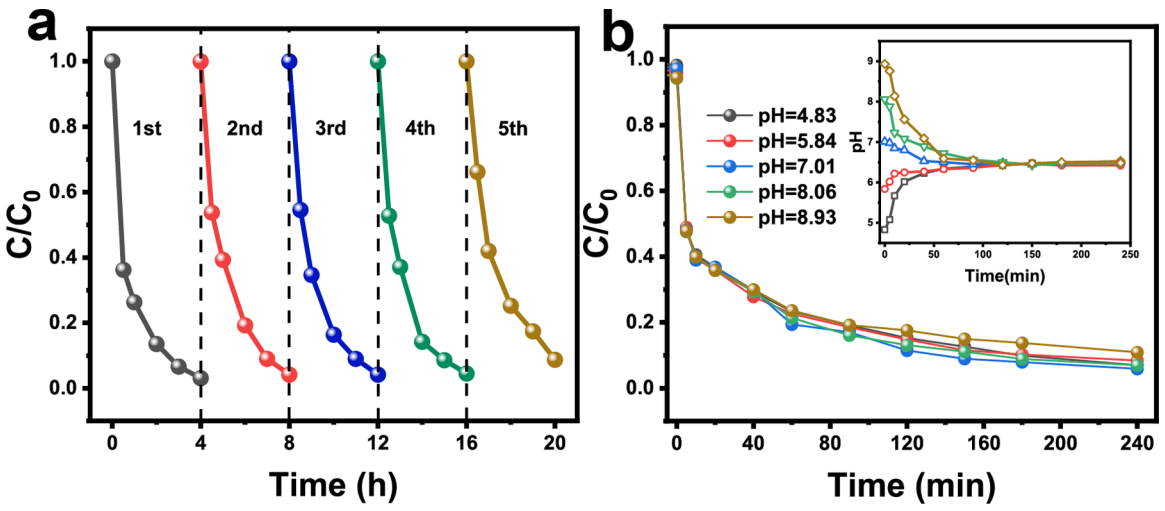

Figure 8. (a) Cycling tests for the degradation of FF, (b) the initial pH value of heterogeneous Fenton-like performance on the degradation of FF by CuNiFeLa-2-LDH (insert: detection of pH value change under different initial pH values).

DOI: 10.1021/acsomega.8b03406
ACS Omega 2019, 4, 1982−1994

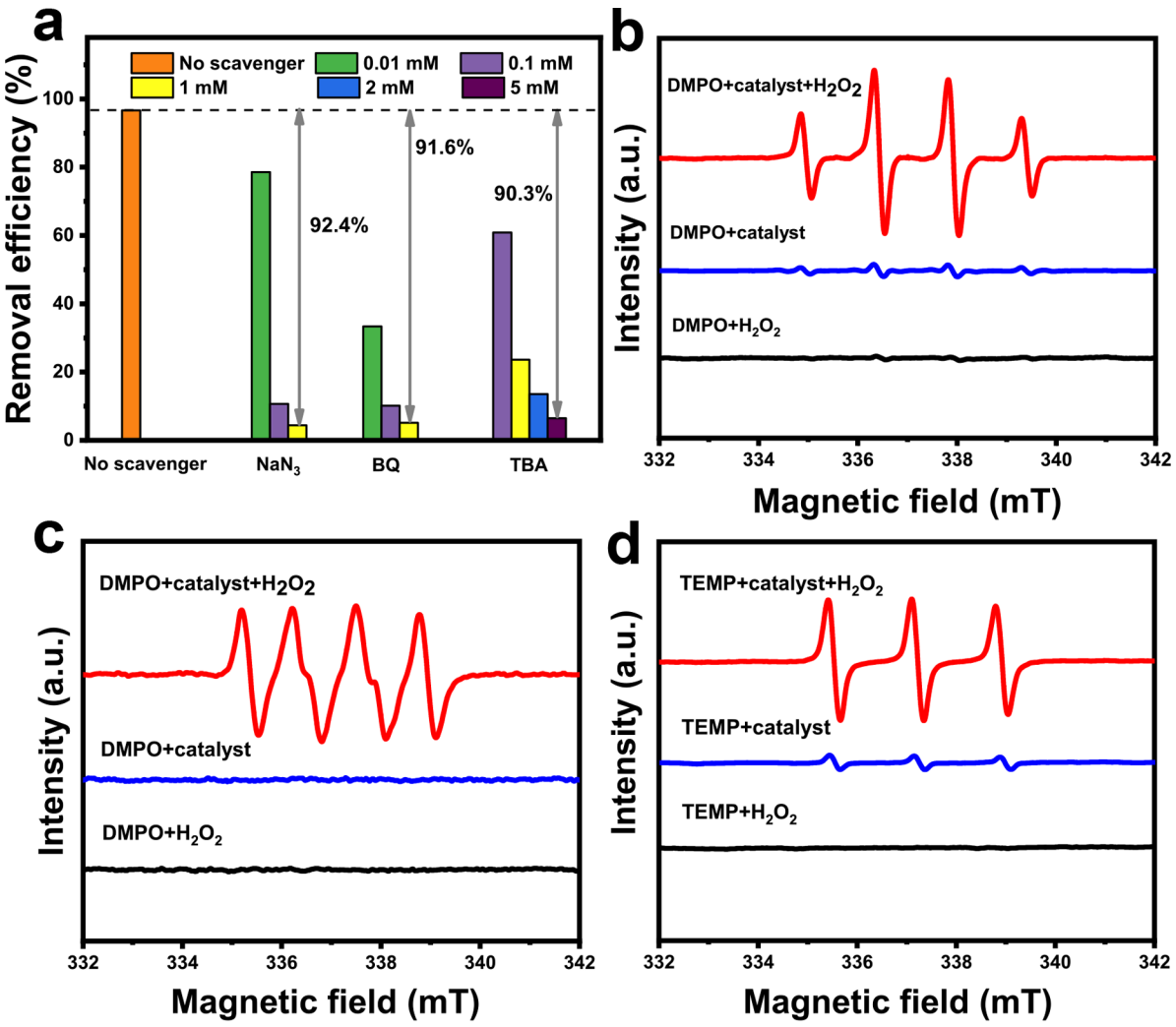

Figure 9. (a) Degradation of FF by CuNiFeLa-2-LDH in the presence of TBA, BQ, and NaN_3 with different concentration gradients. 5,5-Dimethyl-1-pyrroline *N*-oxide (DMPO) or 4-amino-2,2,6,6-tetramethylpiperidine (TEMP) spin trapping electron spin resonance (ESR) spectra for (b) $^{\bullet}OH$ in aqueous suspensions, (c) $HO_2^{\bullet}/^{\bullet}O_2^-$ in dimethyl sulfoxide (DMSO) dispersions, (d) O_2^1 in aqueous suspensions with and without CuNiFeLa-2-LDH or H_2O_2.

As shown in Figure 9b, the signal of four quintessential strong characteristic peaks of DMPO−$^{\bullet}OH$ was detected with the ratio of 1:2:2:1 in the presence of the catalyst and H_2O_2 in aqueous suspension. Because only the catalyst or H_2O_2 existed in aqueous suspensions, the $^{\bullet}OH$ signals was hardly measured by DMPO spin trapping. A similar phenomenon also appeared in the generation of $^{\bullet}O_2^-$ as depicted in Figure 9c. It was clearly observed that the characteristic peaks of DMPO−$^{\bullet}O_2^-$ were detected in DMSO dispersions over CuNiFeLa-2-LDH with H_2O_2. In the situation of H_2O_2 or catalyst isolated, the peaks of $^{\bullet}O_2^-$ did not appear. The signals of O_2^1 were detected by TEMP spin trapping according to Figure 9d. It exhibited three characteristic 1:1:1 triplet peaks which are in correspondence with previous reports,[46,47] indicating the generation of O_2^1 during the reaction process. However, the slight peak value was also detected without the catalyst in this detection, which can be explained by the production from dissolved oxygen.[48] The above facts further implied that $^{\bullet}OH$, $^{\bullet}O_2^-$, and O_2^1 were regenerated and played vital roles as active species in this heterogeneous Fenton-like reaction, which evidenced that H_2O_2 was predominantly reduced as well as oxidized in the presence of CuNiFeLa-2-LDH.

In addition, the PL spectra were implemented to reflect the amount of $^{\bullet}OH$ generated in the process. It was reported that benzoic acid reacted with $^{\bullet}OH$, which can produce fluorescent substance hydroxybenzoic acid.[49] The hydroxybenzoic acid with fluorescent signals can be measured by photoluminescence (PL) spectroscopy, and the amount of $^{\bullet}OH$ was quantified by the PL intensity. Figure 10a shows the PL spectra on the degradation of FF with the excitation wavelength at 316 nm under different reaction conditions. Compared to the absence of the catalyst and H_2O_2, it was obviously observed that a large amount of hydroxyl groups was produced in the solution with the addition of CuNiFeLa-2-LDH. The inset manifested that the amount of hydroxyl groups intensified as the reaction time increased at an emission wavelength of 416 nm. It further illustrated that the production of the active species of the system is attributed to the interaction of the catalyst and H_2O_2.

Figure 5a has shown that the coexistence of Cu and Ni in LDHs can activate H_2O_2 to degrade FF, possibly for the promotion of the electron transfer. Meanwhile, La doping can improve the oxidation between the pollutant and the catalyst. To verify these above analyses, the electrochemical impedance

DOI: 10.1021/acsomega.8b03406
ACS Omega 2019, 4, 1982−1994

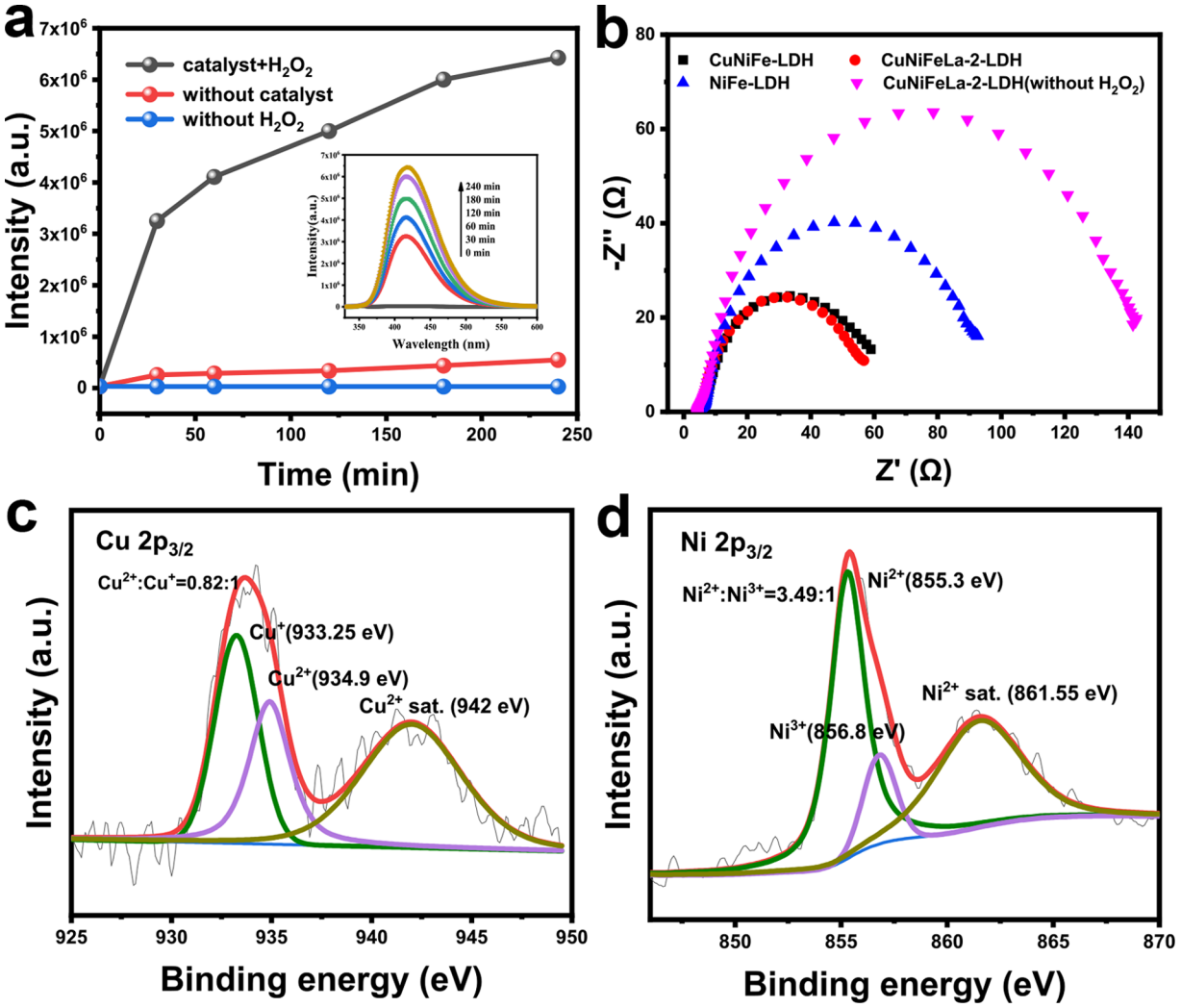

Figure 10. (a) Changes of the PL intensities under different reaction conditions in 10 mM benzoic acid solution (the inset represents the changes of PL intensities with the increased reaction time). (b) Electrochemical impedance spectroscopy (EIS) spectrum of different materials. The high-resolution XPS spectrum of (c) Cu 2p and (d) Ni 2p after the reaction.

spectroscopy (EIS) Nyquist plots was performed to evaluate the electron transfer rate between metals ions. Generally, the narrow arcs of EIS spectra represent the faster electron transfer rate. As shown in Figure 10b, the size of the arcs followed the order of CuNiFeLa-2-LDH < CuNiFe-LDH < NiFe-LDH < CuNiFeLa-2-LDH (without H_2O_2), which illustrated that the addition of Ni and La further accelerated the electron transfer rate in the experimental procedure. Moreover, the high-resolution XPS spectrum of Cu and Ni after the reaction was investigated. As presented in Figure 10c,d, the atomic ratios of Cu^{2+}/Cu^{+} and Ni^{2+}/Ni^{3+} were changed after the reaction. The proportion of Cu^{2+}/Cu^{+} equals to 0.82:1 which is much lower than that of the ratio before the reaction (Cu^{2+}/Cu^{+} = 2.58:1). The increased Cu^{+} composition further confirmed the possible electron transfer from Ni^{2+} to Cu^{2+}.

Therefore, based on the above results, the possible mechanisms for the degradation of FF by the CuNiFeLa-2-LDH catalyst are proposed. First, the layered structure of hydrotalcite-like LDH provides more active sites for the degradation of pollutants in this Cu-dominated Fenton-like reaction. Second, a large number of Ni^{2+} on the catalyst surface with the unique electronic structure can transfer electrons to Cu^{2+} to produce more Cu^{+} through the M−O−M structure in the LDH lattice, which is better for the Fenton-like reaction, because the reaction rate constant of $Cu^{+}-H_2O_2$ (1×10^4 M^{-1} S^{-1}) is higher than $Cu^{2+}-H_2O_2$ (4.6×10^2 M^{-1} S^{-1}). The Cu^{+} can directly react with H_2O_2 to produce hydroxyl radicals. The accelerated cycle of Cu^{2+}/Cu^{+} promoted the production of ROS. Third, the La_2O_3 existing in the layer of CuNiFeLa-2-LDH, which was confirmed by XPS analysis, can provide Lewis basic and Lewis acidic sites simultaneously. Besides, its surface lattice oxygen provides Lewis basic sites, whereas metal ions provide Lewis acidic sites.[50,51] Lewis acids can act as catalysts to promote the oxidation between the substrates and oxidants, further to accelerate the electron transfer rate and enhance the catalytic effect in this Fenton-like reaction system.[52] In addition, the La doping fabricated more mesopores in the material and showed a large specific surface area, making the entrance of FF into the sample more easy. Fourth, the production of $^{\bullet}OH$, $^{\bullet}O_2^{-}$, and O_2^{1} reactive species were ascribed to the interaction of CuNiFeLa-2-LDH and H_2O_2, which can directly attack FF further to oxidize it. However, Fe^{3+} in the brucite-like sheets may not act as the main Fenton-like activity metal ions according to the poor performance of NiFe-LDH on FF degradation. It can be explained by the lower reaction rate of $Fe^{3+}-H_2O_2$ ($(1-2) \times 10^{-2}$ M^{-1} S^{-1})

DOI: 10.1021/acsomega.8b03406
ACS Omega 2019, 4, 1982−1994

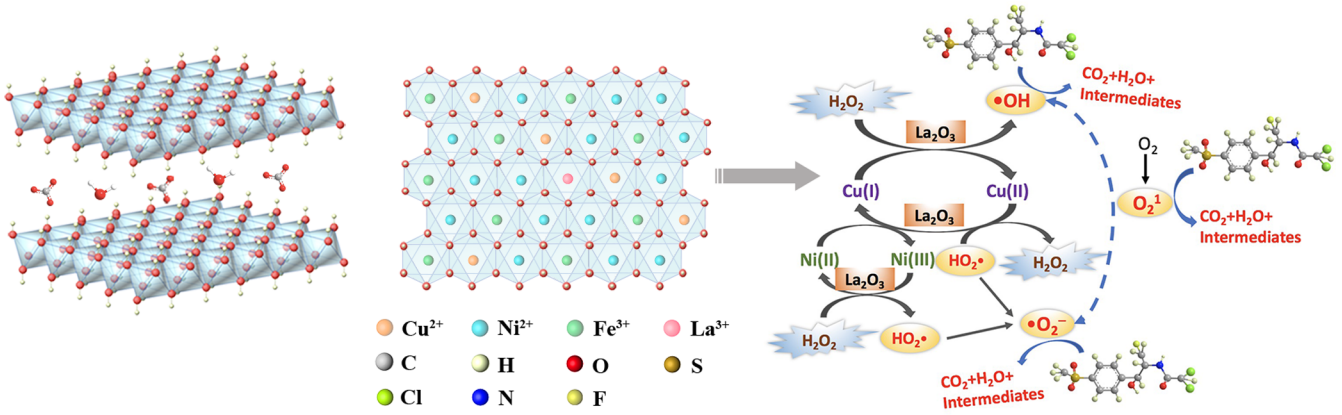

Figure 11. Schematic illustration of the possible mechanism for FF degradation by CuNiFeLa-2-LDH with H_2O_2.

compared with Cu^{2+}−H_2O_2 (1×10^4 M^{-1} S^{-1}). Therefore, the role of Fe^{3+} in this Fenton system can be ignored and it is mainly used for maintaining the layered structure of LDHs. According to the above discussion, the schematic illustration of the possible mechanism is depicted in Figure 11. The reaction procedure between CuNiFeLa-2-LDH and H_2O_2 was explored and presented in the following steps. An electron was transferred from Ni^{2+} to Cu^{2+} which can produce more Cu^+ through the M−O−M structure (eq 5). The reaction between Cu^{2+}/Cu^+ and H_2O_2 engender $HO_2^•$ and $^•OH$ (eqs 6 and 7).[53] The high redox potential of Ni^{3+}/Ni^{2+} can also oxidize H_2O_2 to produce $HO_2^•$ (eq 8).[54] Meanwhile, $HO_2^•$ can break down into $^•O_2^-$ (eq 9) and further produce inefficient O_2 (eq 10). Besides, the production of O_2^1 might be acquired from two aspects. First, the redox potential of $^•OH/OH^-$ ($E^0(^•OH/OH^-)$ = 1.99 eV) is more positive than that of $O_2^1/^•O_2^-$ ($E^0(O_2^1/^•O_2^-)$ = 0.97 eV),[55] resulting in the generation of O_2^1 between radicals, which is consistent with scavenger experiments (eq 11). Second, the dissolved oxygen may participate in the production of O_2^1 according to ESR analysis (eq 12). The existence of La^{3+} can accelerate the electron transfer rate and enhance the catalytic activity. After that, the generation of $^•OH$, $^•O_2^-$, and O_2^1 with high oxidation activity can attack FF in the aqueous solution (eq 13).

$$Cu^{2+} + Ni^{2+} \rightarrow Cu^+ + Ni^{3+} \quad (5)$$

$$Cu^{2+} + H_2O_2 \rightarrow Cu^+ + HO_2^• + H^+ \quad (6)$$

$$Cu^+ + H_2O_2 \rightarrow Cu^{2+} + ^•OH + OH^- \quad (7)$$

$$Ni^{3+} + H_2O_2 \rightarrow Ni^{2+} + HO_2^• + H^+ \quad (8)$$

$$HO_2^• \rightarrow H^+ + ^•O_2^- \quad (9)$$

$$Cu^{2+} + HO_2^• \rightarrow Cu^+ + O_2 + H^+ \quad (10)$$

$$^•O_2^- + ^•OH \rightarrow O_2^1 + OH^- \quad (11)$$

$$O_2 \rightarrow O_2^1 \quad (12)$$

$$\text{ROS } (^•OH, ^•O_2^-, O_2^1) + \text{FF} \rightarrow CO_2 + H_2O + \text{degradation products} \quad (13)$$

3. CONCLUSIONS

In summary, a series of novel Cu-based multi-metal CuNiFeLa-LDHs were prepared by a convenient co-precipitation method. The Fenton-like reaction activities of the materials were evaluated by FF degradation tests in the aqueous solution under dark conditions. The results showed that the La-doped CuNiFe-LDH, with the $La^{3+}/(Fe^{3+} + La^{3+})$ = 0.1 and 5 mmol L^{-1} H_2O_2, exhibited high catalytic activity at room temperature and a wide pH range. The removal efficiency of IBE, DCF, and PR can also reach over 95% after 180 min, indicating that it is suitable to degrade different antibiotics in aqueous solution. The enhanced catalytic activity compared to other LDHs was ascribed to the coexistence of Cu^+/Cu^{2+}, Ni^{3+}/Ni^{2+}, and La_2O_3, leading to the typical promotion effect during the reaction process. The introduction of Ni^{2+}/Ni^{3+} into the lattice of LDH can facilitate the electron transfer of Cu^+/Cu^{2+}. The La doping can improve the oxidation between the substrates and oxidants and provide more mesopores and large specific area in the catalyst, resulting in the increased reaction activity sites and the production of $^•OH$, $^•O_2^-$, and O_2^1 species. Moreover, the catalyst was evidenced to have a wide pH adaptability in the range from 5 to 9 and little copper liberation during the reaction, further demonstrating that the CuNiFeLa-LDH material is a promising Fenton-like catalyst with stability and applicability to purify polluted water containing refractory VAs, FF.

4. MATERIALS AND METHODS

4.1. Materials. Cupric nitrate trihydrate ($Cu(NO_3)_2{\cdot}3H_2O$, AR grade), nickel nitrate hexahydrate ($Ni(NO_3)_2{\cdot}6H_2O$, AR grade), iron nitrate nonahydrate ($Fe(NO_3)_3{\cdot}9H_2O$, AR grade), lanthanum nitrate hexahydrate ($La(NO_3)_3{\cdot}6H_2O$, AR grade), hydrogen peroxide (H_2O_2, 30%, w/w), *p*-benzoquinone ($C_6H_4O_2$, CP grade), *tert*-butanol ($C_4H_{10}O$, CP grade), and sodium azide (NaN_3, AR grade) were obtained from Sinopharm Chemical Reagent Co., Ltd (China). Florfenicol ($C_{12}H_{14}Cl_2FNO_4S$, 98%) were purchased from Adamas Reagent. 5,5-Dimethyl-1-pyrroline *N*-oxide (DMPO, $C_6H_{11}NO$, for ESR-spectroscopy) was purchased from Sigma-Aldrich (St. Louis). Dimethyl sulfoxide (DMSO, C_2H_6SO, 99.8%) and 4-amino-2,2,6,6-tetramethylpiperidine (TEMP, $C_9H_{20}N_2$, 98%) were purchased from Aladdin. All required concentrations of the experimental solutions were diluted with ultrapure water produced from a Milli-Q device (18.2 MΩ cm at 25 °C).

DOI: 10.1021/acsomega.8b03406
ACS Omega 2019, 4, 1982−1994

4.2. Synthesis of Cu-Based LDH Materials. A series of CuNiFeLa-LDHs intercalated with carbonate anions were synthesized by the co-precipitation method at room temperature. Briefly, certain amounts of $Cu(NO_3)_2{\cdot}3H_2O$, $Ni(NO_3)_2{\cdot}6H_2O$, $Fe(NO_3)_3{\cdot}9H_2O$, and $La(NO_3)_3{\cdot}6H_2O$ were dissolved in 200 mL ultrapure water (solution A), where the molar ratio of Cu^{2+}/Ni^{2+} = 1:3, M^{2+}/M^{3+} = 2:1, and $La^{3+}/(Fe^{3+} + La^{3+})$ = 0.05, 0.1, 0.2, 0.5, respectively. Another 100 mL solution containing NaOH (0.5 mol L^{-1}) and Na_2CO_3 (0.1 mol L^{-1}) was also prepared (solution B). Then, solutions A and B were simultaneously added dropwise into 100 mL ultrapure water with continuous stirring. The dropping rate was adjusted to keep the solution pH at 9.0 ± 0.2 during the reaction process. After that, the resulting slurry was aged at 40 °C for 24 h. The obtained solution was filtered using 0.45 μm filter membranes and washed with ultrapure water until the supernatant reached a neutral pH value. The acquired solid material was finally dried at 40 °C overnight and then ground into powder. For identification, different products of La-doped materials were donated as CuNiFeLa-1-LDH, CuNiFeLa-2-LDH, CuNiFeLa-3-LDH, and CuNiFeLa-4-LDH, respectively. Above these, CuFe-LDH, CuNiFe-LDH, NiFe-LDH, and CuMgFeLa-LDH were also prepared with the same procedure.

4.3. Characterization of Materials. The metal contents of the materials were determined by inductively coupled plasma optical emission spectrometry (ICP-OES) Agilent 720 (Agilent). The solid structures of these materials were recorded by a D-8 Advance X-ray diffractometer (Bruker-AXS, Germany). The Fourier transfer infrared (FTIR) spectrum was measured by Bruker Tensor37 (Bruker-AXS, Germany) FTIR instrument. The BET surface area, total pore volume, and pore size distribution of the material were determined by the Autosorb-iQ analyzer (Quantachrome). The ζ-potential of the typical sample was measured by using a Zetasizer apparatus (Nano Z, Malvern, U.K.) with pH ranging from 6.0 to 10.0. The surface morphology and element mapping of the catalysts were obtained by using a scanning electron microscope (SEM, Nova nanoSEM 450, FEI, Netherlands) equipped with an energy dispersive spectrometer (EDS) and a transmission electron microscope (TEM, JEM-2011, JEOL, Japan). The electrochemical impedance spectroscopy (EIS) of each sample was performed by using a three-electrode electrochemical cell equipped with a catalyst anode and a platinum wire cathode in a 0.5 mol L^{-1} Na_2SO_4 solution, and regarded the saturated calomel electrode as the reference electrode. The functional groups and related oxidation states on the surface of the materials were characterized with X-ray photoelectron spectroscopy (XPS). The binding energy of C 1s was set at 284.6 eV which is used as the reference for adjusting other peak positions.

4.4. Fenton-like Reaction Experiment. The Fenton-like reaction activities of the materials were evaluated by degrading FF solutions under dark conditions with continuous magnetic stirring. In a typical Fenton-like catalytic procedure, a certain amount of powder was dispersed into 50.0 mL FF solution at room temperature and then the solution was stirred for 30 min to establish the adsorption−desorption equilibrium. After that, a certain amount of H_2O_2 was added to initiate the reaction. At given time intervals, 1.5 mL aliquots were collected from the suspension and filtered with 0.22 μm membranes to remove the filtered solids. The experimental procedure of IBF, DCF, and PR degradation is the same with FF.

4.5. Analytical Methods. The florfenicol concentrations in the filtered aqueous solution were determined by ultra-performance liquid chromatography (UPLC) with an UV−vis photodiode array detector and an ACQUITY UPC^2 BEH C18 column: 100 × 3.0 mm^2, 1.7 μm particle size. The ultrapure water and acetonitrile were used as the mobile phase with the ratio of 70:30 (water/acetonitrile). The detection limit of FF in this UPLC was 50 μg L^{-1}.

To compare the degradation rate of FF with different catalysts, the apparent rate constant was used to quantitate it, which is expressed as k_{app} (min^{-1}).

■ ASSOCIATED CONTENT

Supporting Information

The Supporting Information is available free of charge on the ACS Publications website at DOI: 10.1021/acsomega.8b03406.

Reusability of the catalyst, ROS trapping and ESR measurement explanation; N_2 adsorption−desorption isotherms, ζ-potential analysis figures, partial XPS characterization spectra and the effect of catalyst dosage figures; chemical composition and EDS results of the material (PDF)

■ AUTHOR INFORMATION

Corresponding Author

*E-mail: zzl@tongji.edu.cn. Phone: +86-21-6598 2426. Fax: +86-21-6598 4626.

ORCID

Zhiliang Zhu: 0000-0002-2516-1033

Notes

The authors declare no competing financial interest.

■ ACKNOWLEDGMENTS

This work was supported by the National Science and Technology Major Project of China (Grant No. 2017ZX07201005).

■ REFERENCES

(1) Sarmah, A. K.; Meyer, M. T.; Boxall, A. B. A. A global perspective on the use, sales, exposure pathways, occurrence, fate and effects of veterinary antibiotics (VAs) in the environment. *Chemosphere* **2006**, *65*, 725−759.

(2) Hu, X.; Zhou, Q.; Luo, Y. Occurrence and source analysis of typical veterinary antibiotics in manure, soil, vegetables and groundwater from organic vegetable bases, northern China. *Environ. Pollut.* **2010**, *158*, 2992−2998.

(3) Tasho, R. P.; Shin, W. T.; Cho, J. Y. Acclimatization of *Pisum sativum* L., grown in soil contaminated with veterinary antibiotics, an attribute of dose hormetic response of root metabolites. *Sci. Total Environ.* **2018**, *635*, 364−374.

(4) Zhang, H.; Zhou, Y.; Huang, Y.; Wu, L.; Liu, X.; Luo, Y. Residues and risks of veterinary antibiotics in protected vegetable soils following application of different manures. *Chemosphere* **2016**, *152*, 229−237.

(5) Liu, L.; Liu, C.; Zheng, J.; Huang, X.; Wang, Z.; Liu, Y.; Zhu, G. Elimination of veterinary antibiotics and antibiotic resistance genes from swine wastewater in the vertical flow constructed wetlands. *Chemosphere* **2013**, *91*, 1088−1093.

(6) Chen, J.; Ying, G. G.; Wei, X. D.; Liu, Y. S.; Liu, S. S.; Hu, L. X.; He, L. Y.; Chen, Z. F.; Chen, F. R.; Yang, Y. Q. Removal of antibiotics and antibiotic resistance genes from domestic sewage by constructed wetlands: Effect of flow configuration and plant species. *Sci. Total Environ.* **2016**, *571*, 974−982.

DOI: 10.1021/acsomega.8b03406
ACS Omega 2019, 4, 1982−1994

(7) Wei, R.; Ge, F.; Chen, M.; Wang, R. Occurrence of Ciprofloxacin, Enrofloxacin, and Florfenicol in Animal Wastewater and Water Resources. *J. Environ. Qual.* **2012**, *41*, 1481−1486.
(8) Zhao, H.; Liu, X.; Cao, Z.; Zhan, Y.; Shi, X.; Yang, Y.; Zhou, J.; Xu, J. Adsorption behavior and mechanism of chloramphenicols, sulfonamides, and non-antibiotic pharmaceuticals on multi-walled carbon nanotubes. *J. Hazard. Mater.* **2016**, *310*, 235−245.
(9) Elmolla, E. S.; Chaudhuri, M. Degradation of amoxicillin, ampicillin and cloxacillin antibiotics in aqueous solution by the UV/ZnO photocatalytic process. *J. Hazard. Mater.* **2010**, *173*, 445−449.
(10) Gao, Y.; Li, Y.; Zhang, L.; Huang, H.; Hu, J.; Shah, S. M.; Su, X. Adsorption and removal of tetracycline antibiotics from aqueous solution by graphene oxide. *J. Colloid Interface Sci.* **2012**, *368*, 540−546.
(11) Li, B.; Zhang, T. Biodegradation and Adsorption of Antibiotics in the Activated Sludge Process. *Environ. Sci. Technol.* **2010**, *44*, 3468−3473.
(12) Giri, A. S.; Golder, A. K. Chloramphenicol Degradation in Fenton and Photo-Fenton: Formation of Fe^{2+}-Chloramphenicol Chelate and Reaction Pathways. *Ind. Eng. Chem. Res.* **2014**, *53*, 16196−16203.
(13) Fan, X.; Hao, H.; Shen, X.; Chen, F.; Zhang, J. Removal and degradation pathway study of sulfasalazine with Fenton-like reaction. *J. Hazard. Mater.* **2011**, *190*, 493−500.
(14) Oturan, M. A.; Aaron, J.-J. Advanced Oxidation Processes in Water/Wastewater Treatment: Principles and Applications. A Review. *Crit. Rev. Environ. Sci. Technol.* **2014**, *44*, 2577−2641.
(15) Wang, M.; Shu, Z.; Zhang, L. X.; Fan, X. Q.; Tao, G. J.; Wang, Y. X.; Chen, L. S.; Wu, M. Y.; Shi, J. L. Amorphous Fe^{2+}-rich FeO_x loaded in mesoporous silica as a highly efficient heterogeneous Fenton catalyst. *Dalton Trans.* **2014**, *43*, 9234−9241.
(16) Zhang, L. L.; Xu, D. A.; Hu, C.; Shi, Y. L. Framework Cu-doped $AlPO_4$ as an effective Fenton-like catalyst for bisphenol A degradation. *Appl. Catal., B* **2017**, *207*, 9−16.
(17) Sun, B.; Li, H.; Li, X.; Liu, X.; Zhang, C.; Xu, H.; Zhao, X. S. Degradation of Organic Dyes over Fenton-Like Cu_2O-Cu/C Catalysts. *Ind. Eng. Chem. Res.* **2018**, *57*, 14011−14021.
(18) Wang, Q.; Ma, Y.; Xing, S. Comparative study of Cu-based bimetallic oxides for Fenton-like degradation of organic pollutants. *Chemosphere* **2018**, *203*, 450−456.
(19) Guimaraes, I. R.; Giroto, A.; Oliveira, L. C. A.; Guerreiro, M. C.; Lima, D. Q.; Fabris, J. D. Synthesis and thermal treatment of cu-doped goethite: Oxidation of quinoline through heterogeneous fenton process. *Appl. Catal., B* **2009**, *91*, 581−586.
(20) Yamaguchi, R.; Kurosu, S.; Suzuki, M.; Kawase, Y. Hydroxyl radical generation by zero-valent iron/Cu (ZVI/Cu) bimetallic catalyst in wastewater treatment: Heterogeneous Fenton/Fenton-like reactions by Fenton reagents formed in-situ under oxic conditions. *Chem. Eng. J.* **2018**, *334*, 1537−1549.
(21) Tian, Z.; Li, Q.; Hou, J.; Li, Y.; Ai, S. Highly selective hydrogenation of alpha,beta-unsaturated aldehydes by Pt catalysts supported on Fe-based layered double hydroxides and derived mixed metal oxides. *Catal. Sci. Technol.* **2016**, *6*, 703−707.
(22) Pan, D.; Ge, S. S.; Zhao, J. K.; Shao, Q.; Guo, L.; Zhang, X. C.; Lin, J.; Xu, G. F.; Guo, Z. H. Synthesis, characterization and photocatalytic activity of mixed-metal oxides derived from NiCoFe ternary layered double hydroxides. *Dalton Trans.* **2018**, *47*, 9765−9778.
(23) Chitrakar, R.; Sonoda, A.; Makita, Y.; Hirotsu, T. Calcined Mg-Al Layered Double Hydroxides for Uptake of Trace Levels of Bromate from Aqueous Solution. *Ind. Eng. Chem. Res.* **2011**, *50*, 9280−9285.
(24) Alejandre, A.; Medina, F.; Rodriguez, X.; Salagre, P.; Cesteros, Y.; Sueiras, J. E. Cu/Ni/Al layered double hydroxides as precursors of catalysts for the wet air oxidation of phenol aqueous solutions. *Appl. Catal., B* **2001**, *30*, 195−207.
(25) Lu, H.; Zhu, Z.; Zhang, H.; Zhu, J.; Qiu, Y.; Zhu, L.; Kueppers, S. Fenton-Like Catalysis and Oxidation/Adsorption Performances of Acetaminophen and Arsenic Pollutants in Water on a Multimetal Cu-Zn Fe-LDH. *ACS Appl. Mater. Interfaces* **2016**, *8*, 25343−25352.
(26) Fahel, J.; Kim, S.; Durand, P.; Andre, E.; Carteret, C. Enhanced catalytic oxidation ability of ternary layered double hydroxides for organic pollutants degradation. *Dalton Trans.* **2016**, *45*, 8224−8235.
(27) Zhu, J.; Zhu, Z.; Zhang, H.; Lu, H.; Qiu, Y.; Zhu, L.; Kueppers, S. Enhanced photocatalytic activity of Ce-doped Zn-Al multi-metal oxide composites derived from layered double hydroxide precursors. *J. Colloid Interface Sci.* **2016**, *481*, 144−157.
(28) Rives, V.; Kannan, S. Layered double hydroxides with the hydrotalcite-type structure containing Cu^{2+}, Ni^{2+} and Al^{3+}. *J. Mater. Chem.* **2000**, *10*, 489−495.
(29) Ramírez-Moreno, M. J.; Romero-Ibarra, I. C.; Hernandez-Perez, M. A.; Pfeiffer, H. CO_2 Adsorption at Elevated Pressure and Temperature on Mg-Al Layered Double Hydroxide. *Ind. Eng. Chem. Res.* **2014**, *53*, 8087−8094.
(30) Dinari, M.; Momeni, M. M.; Ghayeb, Y. Photodegradation of organic dye by ZnCrLa-layered double hydroxide as visible-light photocatalysts. *J. Mater. Sci.: Mater. Electron.* **2016**, *27*, 9861−9869.
(31) Lee, H. V.; Juan, J. C.; Taufiq-Yap, Y. H. Preparation and application of binary acid−base CaO−La_2O_3 catalyst for biodiesel production. *Renewable Energy* **2015**, *74*, 124−132.
(32) Han, X.; Fang, K.; Zhou, J.; Zhao, L.; Sun, Y. Synthesis of higher alcohols over highly dispersed Cu−Fe based catalysts derived from layered double hydroxides. *J. Colloid Interface Sci.* **2016**, *470*, 162−171.
(33) Wang, J.; Li, Y.; Chen, W.; Peng, J.; Hu, J.; Chen, Z.; Wen, T.; Lu, S.; Chen, Y.; Hayat, T.; Ahmad, B.; Wang, X. The rapid coagulation of graphene oxide on La-doped layered double hydroxides. *Chem. Eng. J.* **2017**, *309*, 445−453.
(34) Cai, J.; Zhao, X.; Zhang, Y.; Zhang, Q.; Pan, B. Enhanced fluoride removal by La-doped Li/Al layered double hydroxides. *J. Colloid Interface Sci.* **2018**, *509*, 353−359.
(35) Wierzbicki, D.; Baran, R.; Debek, R.; Motak, M.; Galvez, M. E.; Grzybek, T.; Da Costa, P.; Glatzel, P. Examination of the influence of La promotion on Ni state in hydrotalcite-derived catalysts under CO_2 methanation reaction conditions: Operando X-ray absorption and emission spectroscopy investigation. *Appl. Catal., B* **2018**, *232*, 409−419.
(36) Li, Y.; Zhang, L.; Xiang, X.; Yan, D.; Li, F. Engineering of ZnCo-layered double hydroxide nanowalls toward high-efficiency electrochemical water oxidation. *J. Mater. Chem. A* **2014**, *2*, 13250−13258.
(37) Jun, H.; Zhiliang, Z.; Hongtao, L.; Yanling, Q. Effect of metal composition in lanthanum-doped ferric-based layered double hydroxides and their calcined products on adsorption of arsenate. *RSC Adv.* **2014**, *4*, No. 5156.
(38) Biesinger, M. C.; Lau, L. W. M.; Gerson, A. R.; Smart, R. S. C. Resolving surface chemical states in XPS analysis of first row transition metals, oxides and hydroxides: Sc, Ti, V, Cu and Zn. *Appl. Surf. Sci.* **2010**, *257*, 887−898.
(39) Wang, H.; Zhang, L.; Hu, C.; Wang, X.; Lyu, L.; Sheng, G. Enhanced degradation of organic pollutants over Cu-doped $LaAlO_3$ perovskite through heterogeneous Fenton-like reactions. *Chem. Eng. J.* **2018**, *332*, 572−581.
(40) Fu, Z.; Hu, J.; Hu, W.; Yang, S.; Luo, Y. Quantitative analysis of Ni^{2+}/Ni^{3+} in $Li[Ni_xMn_yCo_z]O_2$ cathode materials: Non-linear least-squares fitting of XPS spectra. *Appl. Surf. Sci.* **2018**, *441*, 1048−1056.
(41) Yang, D. X.; Jiang, T.; Wu, T. B.; Zhang, P.; Han, H. L.; Han, B. X. Highly selective oxidation of cyclohexene to 2-cyclohexene-1-one in water using molecular oxygen over Fe-Co-g-C_3N_4. *Catal. Sci. Technol.* **2016**, *6*, 193−200.
(42) Reddy, B. M.; Chowdhury, B.; Smirniotis, P. G. An XPS study of La_2O_3 and In_2O_3 influence on the physicochemical properties of MoO_3/TiO_2 catalysts. *Appl. Catal., A* **2001**, *219*, 53−60.
(43) Fida, H.; Zhang, G.; Guo, S.; Naeem, A. Heterogeneous Fenton degradation of organic dyes in batch and fixed bed using La-Fe montmorillonite as catalyst. *J. Colloid Interface Sci.* **2017**, *490*, 859−868.

DOI: 10.1021/acsomega.8b03406
ACS Omega 2019, 4, 1982−1994

(44) Zhang, L.; Nie, Y.; Hu, C.; Qu, J. Enhanced Fenton degradation of Rhodamine B over nanoscaled Cu-doped $LaTiO_3$ perovskite. *Appl. Catal., B* **2012**, *125*, 418−424.
(45) Rusevova, K.; Kopinke, F.-D.; Georgi, A. Nano-sized magnetic iron oxides as catalysts for heterogeneous Fenton-like reactions-Influence of Fe(II)/Fe(III) ratio on catalytic performance. *J. Hazard. Mater.* **2012**, *241*−*242*, 433−440.
(46) Wang, F.; Feng, Y.; Chen, P.; Wang, Y.; Su, Y.; Zhang, Q.; Zeng, Y.; Xie, Z.; Liu, H.; Liu, Y.; Lv, W.; Liu, G. Photocatalytic degradation of fluoroquinolone antibiotics using ordered mesoporous g-C_3N_4 under simulated sunlight irradiation: Kinetics, mechanism, and antibacterial activity elimination. *Appl. Catal., B* **2018**, *227*, 114−122.
(47) Han, S. K.; Hwang, T.-M.; Yoon, Y.; Kang, J.-W. Evidence of singlet oxygen and hydroxyl radical formation in aqueous goethite suspension using spin-trapping electron paramagnetic resonance (EPR). *Chemosphere* **2011**, *84*, 1095−1101.
(48) Zhao, H.; Chen, X.; Li, X.; Shen, C.; Qu, B.; Gao, J.; Chen, J.; Quan, X. Photoinduced formation of reactive oxygen species and electrons from metal oxide-silica nanocomposite: An EPR spin-trapping study. *Appl. Surf. Sci.* **2017**, *416*, 281−287.
(49) Xing, M.; Zhang, J.; Qiu, B.; Tian, B.; Anpo, M.; Che, M. A Brown Mesoporous TiO_{2-x}/MCF Composite with an Extremely High Quantum Yield of Solar Energy Photocatalysis for H_2 Evolution. *Small* **2015**, *11*, 1920−1929.
(50) Manoilova, O. V.; Podkolzin, S. G.; Tope, B.; Lercher, J.; Stangland, E. E.; Goupil, J. M.; Weckhuysen, B. M. Surface acidity and basicity of La_2O_3, LaOCl, and $LaCl_3$ characterized by IR spectroscopy, TPD, and DFT calculations. *J. Phys. Chem. B* **2004**, *108*, 15770−15781.
(51) Valange, S.; Beauchaud, A.; Barrault, J.; Gabelica, Z.; Daturi, M.; Can, F. Lanthanum oxides for the selective synthesis of phytosterol esters: Correlation between catalytic and acid-base properties. *J. Catal.* **2007**, *251*, 113−122.
(52) Corma, A.; Garcia, H. Lewis acids as catalysts in oxidation reactions: From homogeneous to heterogeneous systems. *Chem. Rev.* **2002**, *102*, 3837−3892.
(53) Xu, J.; Li, Y.; Yuan, B.; Shen, C.; Fu, M.; Cui, H.; Sun, W. Large scale preparation of Cu-doped α-FeOOH nanoflowers and their photo-Fenton-like catalytic degradation of diclofenac sodium. *Chem. Eng. J.* **2016**, *291*, 174−183.
(54) Wolfenstine, J.; Allen, J. Ni^{3+}/Ni^{2+} redox potential in $LiNiPO_4$. *J. Power Sources* **2005**, *142*, 389−390.
(55) She, X.; Wu, J.; Xu, H.; Zhong, J.; Wang, Y.; Song, Y.; Nie, K.; Liu, Y.; Yang, Y.; Rodrigues, M.-T. F.; Vajtai, R.; Lou, J.; Du, D.; Li, H.; Ajayan, P. M. High Efficiency Photocatalytic Water Splitting Using 2D alpha-Fe_2O_3/g-C_3N_4 Z-Scheme Catalysts. *Adv. Energy Mater.* **2017**, *7*, No. 1700025.

DOI: 10.1021/acsomega.8b03406
ACS Omega 2019, 4, 1982−1994